Spectroscopic diagnostics of morphological changes arising in thermal processing of polypropylene

Donia Hakoume,[1] Leonid A. Dombrovsky,[2,*] Didier Delaunay,[1] and Benoit Rousseau[1]

[1]PRES LUNAM, CNRS, UMR 6607 LTN, Site de la Chantrerie, Rue Christian Pauc, 44306, Nantes, Cedex 3, France

[2]Joint Institute for High Temperatures, Krasnokazarmennaya 17A, Moscow 111116, Russia

*Corresponding author: donia.hakoume@univ-nantes.fr

Received 5 December 2013; revised 21 March 2014; accepted 24 March 2014;
posted 25 March 2014 (Doc. ID 202489); published 18 April 2014

Polypropylene is considered as a representative thermoplastic matrix for advanced composite materials that have some advantages in various engineering applications. Wide-range infrared optical properties of polypropylene are important for combined heat transfer modeling in these composite materials, which are semitransparent in a considerable part of the whole spectral range. This study is focused on optical properties of polypropylene in the visible and near-infrared ranges because the measurements in these ranges exhibit a stronger effect of the processing temperature used in the material manufacturing. The experimental study is based on spectral measurements of both the normal-hemispherical reflectance and transmittance of polypropylene samples. The main characteristics of volumetric absorption and scattering are identified using the inverse problem solution based on the modified two-flux approximation, which is sufficiently accurate to determine the hemispherical characteristics of the radiation field in the range of the problem parameters. In particular, the effect of a relatively strong scattering is observed at the absorption peaks in the near-infrared range. An approximate theoretical model based on spectroscopic data is developed to estimate morphological changes arising in thermal processing of polypropylene at different temperatures.

OCIS codes: (160.5470) Polymers; (290.4020) Mie theory.
http://dx.doi.org/10.1364/AO.53.002702

1. Introduction

In the last three decades, much attention has been paid to the development of new composite materials for various applications, especially in aerospace and transportation [1–3]. In particular, thermoplastic composites (TPCs) have a number of advantages over traditional thermoset composites due to improved fracture toughness, the potential for repeated recycling, and, most notably, possible welding to reshape or remold the product at elevated temperatures. There are several methods used to produce TPC materials [3]. The present study is concerned with the materials processed in infrared ovens [4–6]. A correct choice of the thermal processing parameters should be based on heat transfer models and the infrared properties of materials [7]. At the same time, the wide infrared range, which is really important for heat transfer modeling, is not so informative for analysis of fine elements of the material structure. Therefore, this paper is focused on the short-wave range where polypropylene is a weakly absorbing material and the radiation wavelength is comparable with the size of some important submicrometer elements of the material structure.

The objective of the present study is twofold: (1) to retrieve the main volumetric characteristics of absorption and scattering of radiation in the visible and near-infrared ranges where these properties are sensitive to the material morphology, and (2) to develop an approximate theoretical model, which enables one to estimate morphological changes in polypropylene during thermal processing at different

1559-128X/14/122702-09$15.00/0

temperatures with the use of short-wave spectral measurements.

It should be recalled that semi-crystalline polymers are characterized by a specific microscopic texturing. In this work, the term texture stands for the spatial arrangement of the heterogeneities within the host solid matrix as their respective size, orientation, and shape distributions [8]. It is interesting that some important parameters of the polypropylene texture can be really estimated on the basis of a theoretical analysis of the retrieved spectral behavior of absorption and scattering properties in the visible and infrared spectral ranges.

2. Samples and Experimental Procedure

The samples of polypropylene were designed by an injection process. One processing parameter was varied in the study: the temperature of the mold in production of the samples, which were in the form of a thin square plate (60 mm × 60 mm × 3 mm). A commercial homopolymer of polypropylene Roving Twintex PP from FGI, Amsterdam, New York, USA, was chosen for the sample preparation [melt flow index (MFI) = 4 g/min for 2.16 kg total mass at 230°C]. The material was injected in a SANDRETTO injection press. This is one of the most common techniques in the production of ordinary and advanced materials [9]. The melt temperature was equal to 220°C, the hold pressure at the nozzle was 80 MPa, and the holding time and the total cooling time were 15 and 20 s, respectively. The injection-molding process consists of five major steps. In the first step, the raw material is fed into the heated barrel, where it is melted and mixed to form a homogeneous melt with a constant temperature. The melt is then injected into the mold to fill the cavity. Once the mold is filled, a holding pressure will be exerted to force additional material into the cavity to compensate for the subsequent shrinkage of the product. As soon as the gate freezes, no more packing is needed and the material cools down further, thus lowering the pressure inside the cavity. The part is ejected after complete solidification of the material.

It is interesting to study the effect of the mold temperature on both the texture and optical properties of the produced material. Due to the thermomechanical conditions of the polymer processing, macromolecules in injection-molded material exhibit a local order. The arising spherulites are spherical semi-crystalline regions inside nonbranched linear polymers. Their formation is controlled by several parameters, such as the number of nucleation sites, the structure of the polymer molecules, and the cooling rate. Depending on these parameters, the spherulite diameter may vary in a wide range from a few micrometers to millimeters. The resulting morphology is characterized by the so-called crystallinity, which is usually specified as a percentage of the volume of the material that is crystalline. In the case of polypropylene, the degree of crystallinity is usually about 60%. Note that the term "morphology,"

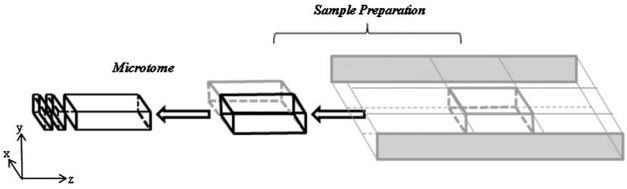

Fig. 1. Cutting procedures followed to obtain the slices for microscopy.

which literally means "the study of the form," also includes the dimensions, shape, size distribution, and orientation of the crystallites. Structural and morphological characterization of the injection-molded polypropylene has attracted the interest of many researchers, for example [10–14]. The experimental observations showed a specific regular crystallite microstructure of semi-crystalline polymers. The samples studied in this paper are thin slices cut using a Leice slit microtome from the middle of the molded slabs produced at the processing temperatures $T_{pr} = 40°C$, 60°C, 80°C, 100°C, and 120°C along the flow (z) direction and parallel to the cross section (x, y) plane (see Fig. 1). In order to observe the morphology changes with the mold temperature, a polarized light optical microscopy Olympus BX61 was used. As expected, it was found that the average diameter of spherulites increases from about 34 to 56 μm with the increase of mold temperature.

To obtain more information on morphology changes with the mold temperature, another study was conducted, which shows that the spherulite diameter at processing temperature 120°C is about 56 μm. Polarized optical microscopy with a LINKAM TMS94 hot stage provided from Likam Scientific Instuments, UK, was used. The growth rate of spherulitic was measured on thin films of thickness 30 μm, which are prepared by pressing the film between two cover glasses at 220°C. After that, the samples were held at 220°C for 4 min on the hot plate in order to remove the effects of the preliminary thermal treatment. Finally, the samples were cooled to crystallize the polymer at $T_{pr} = 120°C$. Several photographs were taken during the crystallization.

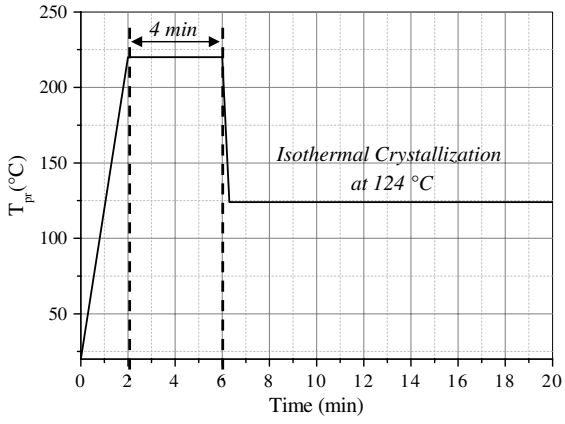

Fig. 2. Diagram of the temperature cycle.

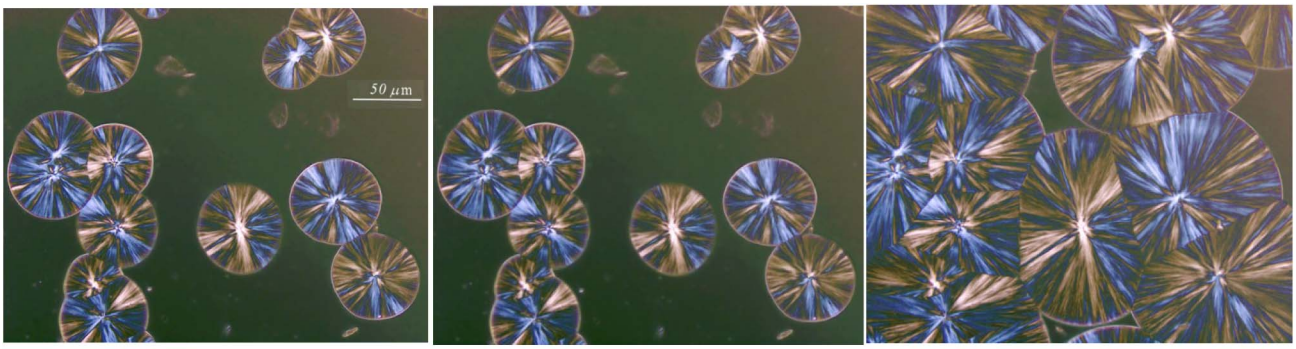

Fig. 3. Microphotograph of typical spherulites in the polypropylene sample during isothermal crystallization at $T_{pr} = 120°C$: (a) $t = 23$ s, (b) 54 s, and (c) 105 s.

The representative parts of these pictures are shown in Fig. 3. One can see that spherulites of various sizes are really almost spherical, and these spherulites grow with time during the isothermal crystallization. This enables us to estimate the rate of growth of spherulite G (m/s) from the Hoffman–Lauritzen relation (see paper [14] for more details on various kinetic theories):

$$K_{av} = \frac{4}{3} N_0 G^{n_{av}}, \tag{1}$$

where N_0 is the number of active germs. Isothermal crystallization experiments to calculate the Avrami constants K_{av} and n_{av} [15–17] were performed by using the TA Q200 calorimeter (Differential scanning calorimetry). This calorimeter was first calibrated in temperature and heat flow. Slices of 7.36 mg mass of PP pellets (from FGI) were placed in an aluminum sample pan and held at 220°C for 4 min to remove possible effects of previous thermal treatment. The sample was then cooled down at the maximum cooling rate to the crystallization temperature $T_{pr} = 124°C$ (see Fig. 2). In our case, we observed an instantaneous germination. In other words, spherulites appeared practically simultaneously. The calculation of the Avrami exponent gives $n_{av} = 2.92$. In the case of instantaneous germination, the latter value is very close to the theoretically predicted value for ideally spherical spherulites (see Table 1). Figure 3 confirms that spherulites of various sizes are really almost spherical. One can calculate the Avrami constant using the data of Fig. 3. The resulting values of other parameters are $G = 1.01$ μm/s and $N_0 = 2.2 \cdot 10^{11}$ m^{-3}. The calculated average diameter of the spherulite at $T_{pr} = 124°C$ is 62 μm. The latter value is in good agreement with the experimental observations.

Table 1. Value of Avrami Exponent Depending on the Geometry and Germination

Shape of Spherulites	Sporadic Germination	Instantaneous Germination
Spherical	4	3
Disc	3	2
Sticks	2	1

The spectral values of directional-hemispherical transmittance and reflectance were measured using Fourier spectrometer Bruker Vertex 80V from Bruker Optics, Germany, equipped with a PTFE integrating sphere (75 mm diameter). The experimental technique of this type is widely used in studies of semitransparent dispersed materials. Therefore, we do not reproduce here the experimental setup schematics, which can be found elsewhere [18–21]. The spectral measurements in the wavelength range of $0.67 \le \lambda \le 1.1$ μm are analyzed in this paper.

It is natural to assume that the polypropylene morphology can be not uniform across the sample. This sample's asymmetry is related with specific conditions of cooling when the stage of crystallization has finished. The term "orientation" is attributed to illumination of two opposite sides of the sample, which is simply rotated 180°C within the spectrometer. The measurements of both normal-hemispherical reflectance and transmittance for two different orientations of each sample were made with subsequent separate identification of the volume-averaged optical properties of the samples.

3. Experimental Results and Preliminary Analysis

The measurements were made in a short-wave spectral range of polypropylene semi-transparency at different orientations of five samples of polypropylene produced at different processing temperatures. The measurements for two different orientations of each sample are presented in Fig. 4. One can see that both the normal-hemispherical reflectance and transmittance are really dependent on the sample orientation. A detailed analysis of the optical properties of all the samples will be given below. At the same time, the principal problem of a relative contribution of surface and volumetric effects can be solved on the basis of a preliminary analysis for one selected sample. Sample 1 was selected for this analysis.

For a preliminary analysis of these data, it is convenient to introduce the value of normal absorbance,

$$A_n = 1 - R_{n-h} - T_{n-h}, \tag{2}$$

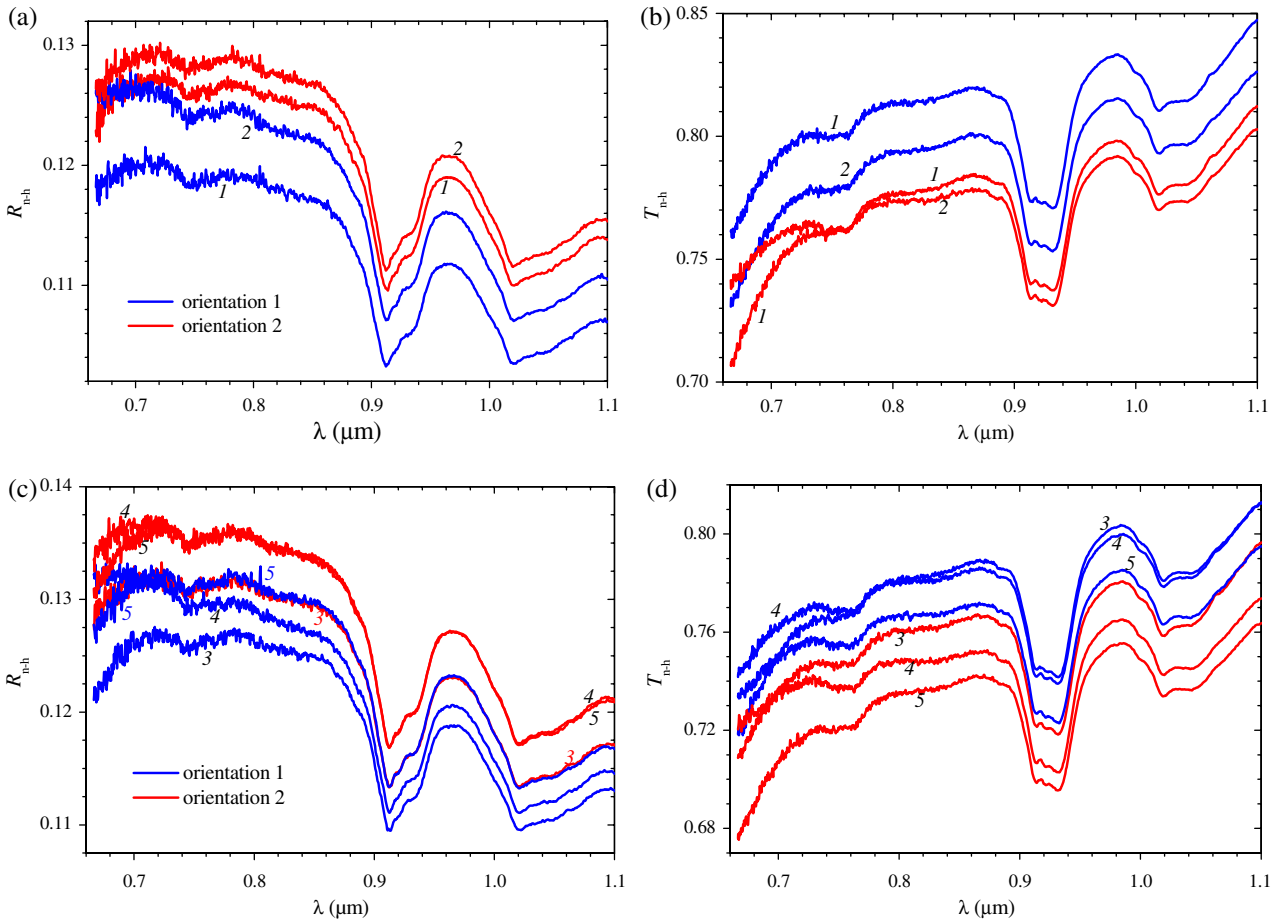

Fig. 4. Measured normal-hemispherical (a), (c) reflectance and (b), (d) transmittance at different orientations of the samples: 1, $T_{pr} = 40°C$; 2, 60°C;, 3, 80°C; 4, 100°C; and 5, 120°C.

and consider the results for sample 1 (at $T_{pr} = 40°C$) presented in Table 2. One can see that the "second" orientation of the sample is characterized by 0.9%–1.0% greater reflectance. The quantitative effect is almost the same at different wavelengths. There are two possible explanations for this effect: the simplest one is an additional scattering by a slightly rough surface of the sample (the opposite surface looks much smoother), and the second one is a stronger volumetric scattering by a surface layer near the irradiated side of the sample in the case of orientation 2. If the effect of a rough surface is predominant (this version seems to be not realistic for the range of semi-transparency), both transmittance and absorbance of the sample decrease during the turn from orientation 1 to orientation 2. But this is not the case (see Fig. 4 and Table 2): the absorbance is increased by 1.1%–1.4%! This means that the first hypothesis is not true and the effect of relatively strong volumetric scattering near the irradiated surface in the case of the second orientation of the samples is observed. A stronger volumetric scattering of radiation near the irradiated surface in the case of the second orientation leads to an increase in both reflectance and absorbance and decreases the sample transmittance. The resulting effect on transmittance is considerable: it is about 2.0%–2.4% (see Table 2). This may be a result of nonsymmetric conditions of the sample cooling.

Obviously, there is no physical sense in averaging the primary data for two different orientations of the sample. The correct way to determine volume-averaged optical properties of inhomogeneous samples is an averaging of the optical properties

Table 2. Effect of the Sample 1 Orientation on Reflectance, Transmittance, and Absorbance

$\lambda = 0.7$ μm			$\lambda = 0.9$ μm		
Reflectance	Transmittance	Absorbance	Reflectance	Transmittance	Absorbance
$R_{n-h}^{(1)} = 11.8\%$	$T_{n-h}^{(1)} = 78.1\%$	$A_n^{(1)} = 10.1\%$	$R_{n-h}^{(1)} = 10.8\%$	$T_{n-h}^{(1)} = 80.3\%$	$A_n^{(1)} = 8.9\%$
$R_{n-h}^{(2)} = 12.8\%$	$T_{n-h}^{(2)} = 75.7\%$	$A_n^{(2)} = 11.5\%$	$R_{n-h}^{(2)} = 11.7\%$	$T_{n-h}^{(2)} = 78.3\%$	$A_n^{(2)} = 10.0\%$
$R_{n-h}^{(2)} - R_{n-h}^{(1)} = 1.0\%$	$T_{n-h}^{(2)} - T_{n-h}^{(1)} = -2.4\%$	$A_n^{(2)} - A_n^{(1)} = 1.4\%$	$R_{n-h}^{(2)} - R_{n-h}^{(1)} = 0.9\%$	$T_{n-h}^{(2)} - T_{n-h}^{(1)} = -2.0\%$	$A_n^{(2)} - A_n^{(1)} = 1.1\%$

retrieved from the measurements for two different orientations of the sample.

4. Identification of Optical Properties

In this paper, the identification procedure is based on transport approximation of the scattering phase function and the modified two-flux approximation [22–24], which takes into account the effect of total internal reflection at the interfaces. For the reader's convenience, the analytical solution for normal-hemispherical reflectance R_{n-h} and transmittance T_{n-h} obtained with the use of the modified two-flux approximation is reproduced below:

$$R_{n-h} = R^0_{n-h} + D(1 + B/\zeta + C)$$
$$T_{n-h} = T^0_{n-h} + D[A/\zeta + (1 + \rho_n)E], \quad (3a)$$

$$R^0_{n-h} = \rho_n + \frac{(1-\rho_n)^2 C}{1-\rho_n C} \qquad T^0_{n-h} = \frac{(1-\rho_n)^2}{1-\rho_n C} E$$
$$C = \rho_n E^2 \qquad E = \exp(-\tau^0_{tr}), \quad (3b)$$

$$A = \frac{k_1(\varphi s + c)E + k_2}{(1+\varphi^2)s + 2\varphi c} \qquad B = \frac{k_1 E + k_2(\varphi s + c)}{(1+\varphi^2)s + 2\varphi c}$$
$$D = \frac{2\gamma\omega_{tr}}{\zeta^2 - 1}\frac{1-\rho_n}{1-\rho_n C}, \quad (3c)$$

$$k_1 = (1-2\gamma) - (1+2\gamma)\rho_n$$
$$k_2 = (1-2\gamma)C - (1+2\gamma), \quad (3d)$$

$$\varphi = 2\gamma/\zeta \qquad \gamma = (1-\rho_n)/(1+\rho_n)$$
$$\zeta^2 = 4(1-\omega_{tr}) \qquad \rho_n = (n-1)^2/(n+1)^2, \quad (3e)$$

$$s = \sinh(\zeta\tau^0_{tr}) \qquad c = \cosh(\zeta\tau^0_{tr}), \quad (3f)$$

where the values of R^0_{n-h} and T^0_{n-h} correspond to a contribution of the collimated component of the radiation field, ρ_n is the normal reflectivity of the interfaces, $\tau^0_{tr} = \beta_{tr} d$ is the transport optical thickness of the sample of thickness d, $\beta_{tr} = \alpha + \sigma_{tr}$ is the transport extinction coefficient, α is the absorption coefficient, σ_{tr} is the transport scattering coefficient, and $\omega_{tr} = \sigma_{tr}/\beta_{tr}$ is the transport albedo of the medium. Of course, the coefficients in Eq. (3) are spectrally dependent, but the corresponding subscripts are omitted for brevity. It should be noted that the singularity in Eq. (3c) at the eigenvalue $\zeta = 1$ does not lead to additional difficulties because it is sufficient to use the solution for $\zeta \neq 1$ in practical calculations.

Note that the normal reflectivity ρ_n is used in the above analytical solution not only for collimated radiation but also for the diffuse radiation component, as was done in [22]. It is not quite correct, and a more accurate solution should be based on averaging of the reflectance recommended in [25]. It was shown in [26] by comparison with the exact numerical solutions that this correction improves the results in the case of a strongly refracting medium. But there is no need in this correction for the particular problem under consideration.

The inverse problem solution with the use of analytical solution [Eqs. (3a)–(3f)] is not mathematically difficult, and there is no need to discuss a simple computational procedure [22]. The resulting spectral dependences of the absorption coefficient and transport scattering coefficient after arithmetic averaging of the volumetric optical properties retrieved from the measurements for two different orientations of the sample are presented in Fig. 5. The calculations were conducted at an approximate constant value of index of refraction $n = 1.5$ [27] because both α and σ_{tr} are weakly sensitive to small variations of the refractive index.

5. Theoretical Analysis

One can see in Fig. 5 that both absorption and transport scattering coefficients are small and the samples are optically thin in the spectral range under consideration. At the same time, the scattering is predominant in the main part of the spectral range.

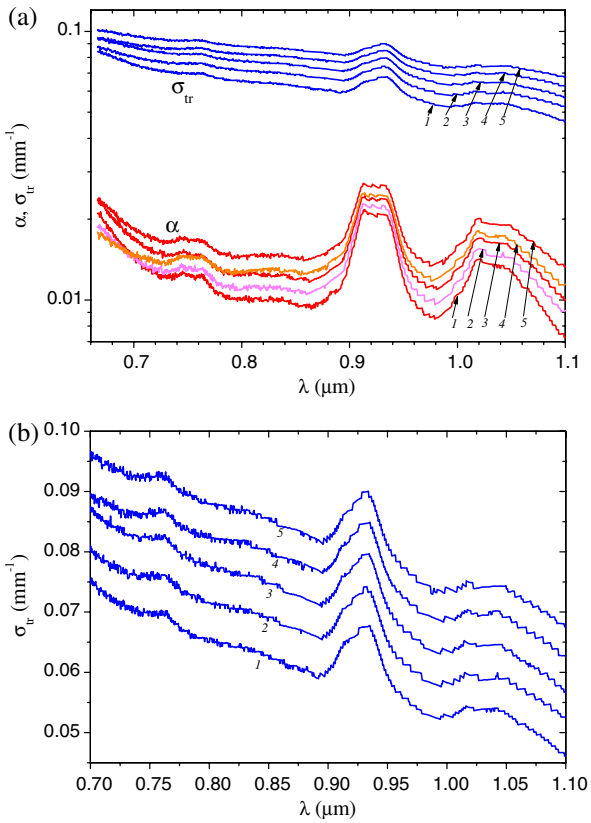

Fig. 5. Averaged absorption coefficient (red curves) and transport scattering coefficient (blue curves): 1, $T_{pr} = 40°C$; 2, 60°C; 3, 80°C; 4, 100°C; and 5, 120°C. The logarithmic scale is used in panel (a) for both values, and the linear scale is used in panel (b) for the scattering data.

A considerable value of σ_{tr} indicates that there are some scattering objects (particles) in the sample, and the characteristic size of these particles is comparable to the wavelength. It should be recalled that only scattering can be used to retrieve some data on the material structure in the case of optically soft dispersed materials. The absorption coefficient of such materials is insensitive to the morphology, and it is simply proportional to the partial volumes of the absorbing substances [28].

The decrease of σ_{tr} with the wavelength is typical for the case in which an average particle size is less than the wavelength [24]. It is important that the curves of $\sigma_{tr}(\lambda)$ for different samples are similar to each other (see the lower panel in Fig. 5). Physically, this means that a geometrical similarity of the scattering objects in polypropylene samples produced at different processing temperatures is proved. Most likely, these scattering particles are randomly oriented lamellas (or the gaps between them), which can be observed in the microphotographs (see Fig. 3).

It is interesting that local maxima of σ_{tr} are observed at the absorption peaks of $\lambda \approx 0.93$ μm and $\lambda \approx 1.04$ μm. It looks similar to a rare effect of the so-called scattering by absorption [24,29]. The physical explanation of the scattering by absorption is quite clear: the local absorption leads to deformation of the wave front even in the case in which there is no spatial variation of the index of refraction. The electromagnetic wave near this local region of more strong absorption does not propagate in the original direction, and this is scattering. It is well known that direct Mie calculations for particles at complex index of refraction $m = 1 - i\kappa$ yield nonzero scattering, which depends on diffraction parameter x and absorption index κ [24]. An effect similar to the scattering by absorption is also observed in the case of particles with a relative index of refraction $\bar{n} \neq 1$ and significant value of a relative index of absorption $\bar{\kappa}$ [24]. This variant will be considered below in the analysis of the optical properties of polypropylene near the absorption peaks.

As to the range between the absorption peaks, it is sufficient to consider the effect of small spatial variation of $\bar{n}$ to explain the observed scattering. Let us consider scattering of radiation by randomly oriented long cylinders to estimate the effect of lamella thickness on spectral dependences of $\sigma_{tr}(\lambda)$. A constant value of the relative index of refraction $\bar{n} = 1.1$ or 1.01 at zero absorption is used in the calculations for the ensemble of independently scattering optically soft lamellas [28,30,31]. The results of Mie theory calculations normalized to the volume fraction of particles, f_v, are presented in Fig. 6. The evolution of spectral dependences from the Rayleigh limit with $\sigma_{tr} \sim \lambda^{-4}$ to the case of large particles, when σ_{tr} is almost constant or even increases with wavelength, is quite clear from Fig. 5. Moreover, the results for different indices of refraction are similar to each other, and the following proportionality takes place for optically soft particles [24]:

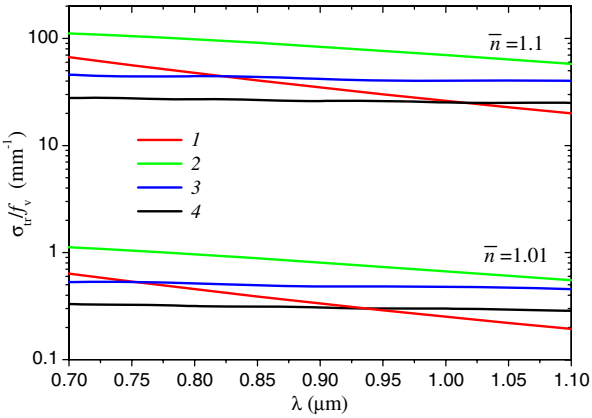

Fig. 6. Transport scattering coefficient of randomly oriented optically soft long cylinders: 1, $a = 0.05$ μm; 2, 0.1 μm; 3, 0.5 μm; and 4, 1 μm.

$$\sigma_{tr} \sim (\bar{n} - 1)^2. \tag{4}$$

Note that the above results are the same for both $\bar{n} > 1$ and $\bar{n} < 1$. This can be confirmed by direct Mie calculations, but is also obvious from the scattering theory for optically soft particles [24,30,31]. According to Fig. 5, the value of σ_{tr} significantly decreases with wavelength in the spectral range considered. One can easily determine that an equivalent radius of scattering particles is about 0.1 μm. The latter conclusion does not depend on the value of $\bar{n}$. A comparison between the Mie theory predictions and experimental data is presented in Fig. 7. The data for processing temperature $T_{pr} = 60°C$ are considered because of a relatively small effect of the sample orientation. One can see that computational results are very sensitive to the value of particle radius, whereas the effect of uncertainty in the relative index of refraction is insignificant. This is very important because it makes possible rather accurate estimates of both the radius and the volume fraction of scattering particles. As one can expect, the volume fraction of particles, which gives good agreement with the experiment, is very sensitive to the relative index

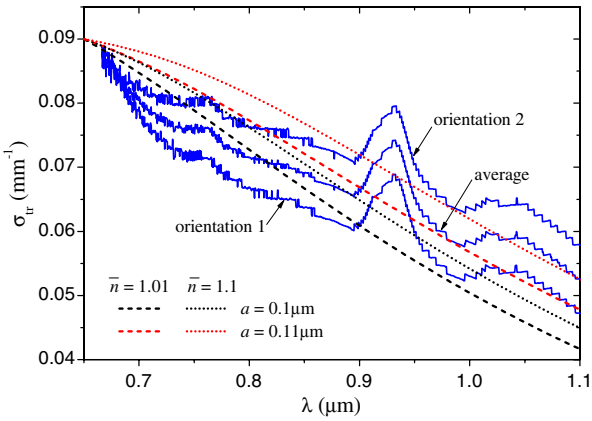

Fig. 7. Transport scattering coefficient for the sample processed at $T_{pr} = 60°C$: solid curves, experiment; dashed curves, calculations for randomly oriented cylinders.

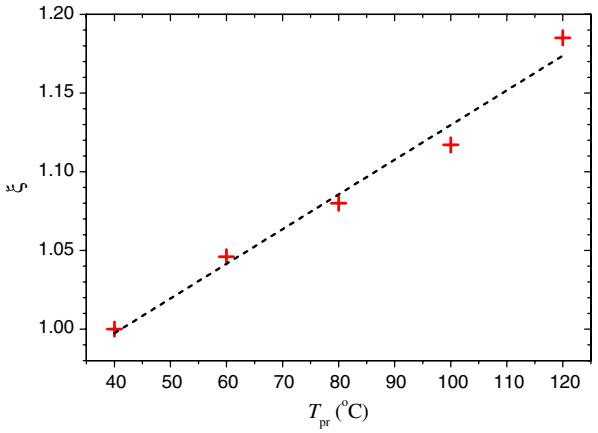

Fig. 8. Increase of the relative volume fraction of scattering particles in polypropylene samples with the processing temperature.

of refraction. In the case of $a = 0.1$ μm, the calculations give

$$f_v \approx 7.6 \cdot 10^{-6}/(\bar{n} - 1)^2. \quad (5)$$

As one can expect, the calculations showed almost linear dependence of the volume fraction of scattering particles on the processing temperature, and the function

$$\xi(T_{pr}) = f_v(T_{pr})/f_v(T_{pr}^0), \qquad T_{pr} > T_{pr}^0 = 40°C \quad (6)$$

is independent of the relative index of refraction of optically soft scattering particles. The calculated values of ξ for polypropylene samples are plotted in Fig. 8, where the fitting linear dependence is also shown. Of course, the error of these calculations may be considerable because of the nonuniformity of the samples and the resulting difference in transport scattering coefficients determined at two orientations of the samples. Nevertheless, it is very interesting that spectroscopic measurements enabled us not only to estimate the size of scattering particles in polypropylene samples but also to quantify the increase of the volume fraction of these particles with the processing temperature.

It is clear that formation of the internal structure of every sample was finished long ago before the experiment because of the cooling stage of the sample preparation. To our mind, this makes it possible to explain a qualitative analogy between the time variation of the sample morphology during thermal processing (see Fig. 3) and the theoretically analyzed variation of the sample morphology with the processing temperature. The latter means that one can use quantitative estimates presented in Fig. 8 to examine the existing data for the kinetics of the crystalline structure formation.

Note that a very strong dependence of the volume fraction of scattering particles on their relative index of refraction makes it possible to estimate the value of $|\bar{n} - 1|$ from the known values of f_v. But this particular task is beyond the scope of this paper.

It is also interesting to consider the resonance scattering at the absorption peaks. This effect is more pronounced at $\lambda \approx 0.93$ μm. An additional scattering of radiation at this wavelength is characterized by the value of $\Delta\sigma_{tr} = 0.022$ at the additional peak absorption about $\Delta\alpha = 0.013$. Both values are exactly the same for all samples and do not depend on variable volume fraction of the above-discussed scattering particles. This means that thin lamellas are not responsible for this additional scattering, and the absorbing particles are quite different from lamella objects. It is unexpected, but the volume fraction of these particles is independent of the processing temperature of polypropylene samples.

Let us assume that these absorbing quasi-particles (this term is used to distinguish these objects from the above-discussed refracting particles) are spherical. This assumption is not principle because the shape of quasi-particles is not expected to be important for further estimates. It is natural to neglect possible effects of dependent scattering [32–34] and use the classical Mie solution [31] for homogeneous spherical quasi-particles of the same radius a_q. It is known from the Mie theory that the efficiency factor of absorption, Q_a, and transport efficiency factor of scattering, Q_s^{tr}, depend on two parameters only. In the case of a refracting and weakly absorbing host medium around the particles, these parameters are the effective diffraction (size) parameter $\bar{x} = 2\pi a_q n/\lambda$ and the relative complex index of refraction of the particle substance $\bar{m}_q = (n_q - i\kappa_q)/n$ [28,35].

It is interesting to consider the following ratio:

$$S = \Delta\sigma_{tr}/\Delta\alpha = Q_s^{tr}/Q_a, \quad (7)$$

which can be determined from the experiment and compared with the Mie scattering calculations. It is clear that the experimental value of $S = 1.17$ cannot be obtained theoretically in the case of optically soft particles ($|\bar{m}_q| \ll 1$) [20]. At the same time, we should consider only very small objects, which are not seen in the image of Fig. 3. After a series of calculations, the hypothesis of the presence of numerous small gas bubbles seems to be realistic. This gas should have a peak of absorption at $\lambda \approx 0.93$ μm. It is interesting that water vapor satisfies the latter condition [36].

The results of Mie calculations presented in Fig. 9 show the resonance behavior of both absorption and scattering efficiency factors for small absorbing bubbles. The positions of the main maxima of $Q_a(\bar{x})$ and $Q_s^{tr}(\bar{x})$ are close to each other, but the maximum value of the scattering ratio $S(\bar{x})$ is slightly shifted to a greater value of the diffraction parameter. In other words, the maximum of S is predicted at a bit shorter wavelength than the absorption peak. Nevertheless, one can see good qualitative agreement between the theoretical estimate and experimental data. This can be treated as an indirect confirmation of the above hypothesis about the effect of small gas bubbles.

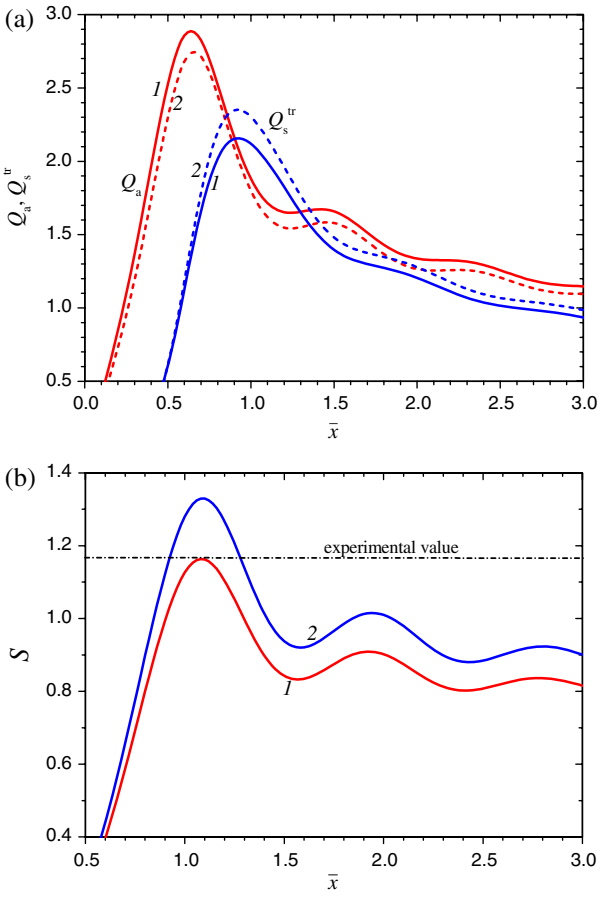

Fig. 9. Optical properties of absorbing gas bubbles in polypropylene predicted by Mie theory at $\bar{m}_q = 0.667 - i\bar{\kappa}_q$, $\bar{\kappa}_q = 1.9$ (*1*) and $\bar{\kappa}_q = 2.0$ (*2*): (a) efficiency factor of absorption and transport efficiency factor of scattering, (b) scattering ratio.

The calculations give the following range for the radius of these gas bubbles: $0.09 < a_q < 0.14$ μm.

To the best of our knowledge, there is no experimental data in the literature about very small gas bubbles in polypropylene, at least in the case of thermal processing like that used in the production of the samples under consideration. Therefore, we are not sure that our preliminary explanation of resonance scattering is really correct. Further experimental studies on fine morphology of polypropylene using electronic microscopy or other special techniques may confirm or disprove our version about microbubbles. But this is beyond the scope of this paper.

6. Conclusions

The visible and near-infrared optical properties of semitransparent polypropylene samples prepared at various processing temperatures from 40°C to 120°C were studied using the measurements of both normal-hemispherical reflectance and transmittance and subsequent identification of the spectral absorption coefficient and transport scattering coefficient of polypropylene.

The analysis of spectral dependences of the transport scattering coefficient for five samples showed that thin randomly oriented lamellas and the narrow gaps between them are responsible for the observed scattering in the spectral range considered (excluding the vicinity of the absorption peaks). The Mie calculations indicated that an average radius of elongated scattering particles is about 0.1 μm, and this value is independent of the processing temperature of polypropylene. At the same time, the volume fraction of scattering particles increases almost linearly with processing temperature. A quantitative parameter that characterizes a degree of the material crystallinity was suggested, and the value of this parameter was determined from the spectroscopic measurements.

The effect of relatively strong scattering at the absorption peaks was observed for polypropylene at the absorption peaks at wavelengths of about 0.93 and 1.04 μm. It was shown that this effect is the same for every sample and it is totally insensitive to the morphological differences between the samples. Moreover, the scattering appears to be so strong that it cannot be explained only by a nonuniform spatial distribution of absorbing particles. The Mie calculations enable the authors to suggest a hypothesis that this effect is produced by numerous small gas bubbles in the material. An average size of these submicrometer bubbles was estimated from comparison of theoretical predictions with experimental data at a wavelength of about 0.93 μm, which practically coincides with a relatively strong absorption peak of water vapor. This preliminary hypothesis may be confirmed or disproved by subsequent direct measurements.

In general, many submicrometer details of the polypropylene morphology can be studied using the analysis of spectroscopic data obtained for polypropylene samples in the visible and infrared ranges.

D. Hakoume acknowledges the French Ministry of Higher Education and Research for supporting this work. D. H. is also grateful to Jalal Faraj, Nicolas Boyard, Jerome Delmas, and Christophe Le Bozec (LTN, Nantes, France) for their kind assistance in preparation and optical characterization of the samples. L. Dombrovsky is grateful to the University of Nantes and the Russian Foundation for Basic Research (Grant No. 13-08-00022-a) for their partial financial support of his participation in this study.

References

1. R. Offringa, "Thermoplastic applications composites-rapid," Composites A: Appl. Sci. Manuf. **27**, 329–336 (1996).
2. D. Hull and T. Clyne, *An Introduction to Composite Materials* (Cambridge University, 1996).
3. T. G. Gutowski, *Advanced Composites Manufacturing* (Wiley, 1997).
4. F. M. Schmidt, Y. Le Maoult, and S. Monteix, "Modelling of infrared heating of thermoplastic sheet used in thermoforming process," J. Mater. Process. Technol. **144**, 225–231 (2003).
5. P. Mallick and S. Newman, *Composite Materials Technology: Process and Properties* (Hanser, 1990).
6. D. Kim, W. I. Lee, and K. Friedrich, "A model for a thermoplastic pultrusion process using commingled yarns," Compos. Sci. Technol. **61**, 1065–1077 (2001).

7. R. Siegel and J. R. Howell, *Thermal Radiation Heat Transfer*, 4th ed. (Taylor & Francis, 2001).
8. B. Rousseau, D. De Sousa Meneses, P. Echegut, and J.-F. Thovert, "Textural parameters influencing the radiative properties of a semitransparent porous media," Int. J. Therm. Sci. **50**, 178–186 (2011).
9. R. Mendoza, G. Régnier, W. Seiler, and J. L. Lebrun, "Spatial distribution of molecular orientation in injection molded iPP: influence of processing conditions," Polymer **44**, 3363–3373 (2003).
10. M. Kantz, J. Newman, and F. Stigale, "The skin-core morphology and structure–property relationships in injection-molded polypropylene," J. Appl. Polym. Sci. **16**, 1249–1260 (1972).
11. G. Menges, G. Wubken, and B. Horn, "Effect of the processing conditions on the crystallinity and morphological structure of partially crystalline injection moldings," Colloid Polym. Sci. **254**, 267–278 (1976).
12. F. Mitsuyoshi, T. Wakino, and Y. Kawasaki, "Structure of skin layer in injection-molded polypropylene," J. Appl. Polym. Sci. **35**, 29–49 (1988).
13. M. Saiu, V. Brucato, S. Piccarolo, and G. Titomanlio, "Injection molding of isotactic polypropylene (iPP). An integrated experimental investigation," Int. Polym. Process. **7**, 267–273 (1992).
14. R. Pantani, I. Coccorullo, V. Speranza, and G. Titomanlia, "Modeling of morphology evolution in the injection molding process of thermoplastic polymers," Prog. Polym. Sci. **30**, 1185–1222 (2005).
15. M. Avrami, "Kinetics of phase change. I General theory," J. Chem. Phys. **7**, 1103–1112 (1939).
16. M. Avrami, "Kinetics of phase change. II Transformation-time relations for random distribution of nuclei," J. Chem. Phys. **8**, 212–224 (1940).
17. M. Avrami, "Granulation, phase change, and microstructure kinetics of phase change III," J. Chem. Phys. **9**, 177–184 (1941).
18. D. Baillis and J.-F. Sacadura, "Thermal radiation properties of dispersed media: theoretical prediction and experimental characterization," J. Quant. Spectrosc. Radiat. Transfer **67**, 327–363 (2000).
19. J.-F. Sacadura and D. Baillis, "Experimental characterization of thermal radiation properties of dispersed media," Int. J. Therm. Sci. **41**, 699–707 (2002).
20. J.-F. Sacadura, "Thermal radiative properties of complex media: theoretical prediction versus experimental identification," Heat Transf. Eng. **32**, 754–770 (2011).
21. L. A. Dombrovsky, B. Rousseau, P. Echegut, J. H. Randrianalisoa, and D. Baillis, "High temperature infrared properties of YSZ electrolyte ceramics for SOFCs: experimental determination and theoretical modeling," J. Am. Ceram. Soc. **94**, 4310–4316 (2011).
22. L. A. Dombrovsky, J. Randrianalisoa, and D. Baillis, "Modified two-flux approximation for identification of radiative properties of absorbing and scattering media from directional-hemispherical measurements," J. Opt. Soc. Am. A **23**, 91–98 (2006).
23. L. A. Dombrovsky, "The use of approximation and diffusion-based models in radiative transfer calculations," Comput. Therm. Sci. **4**, 297–315 (2012).
24. L. A. Dombrovsky and D. Baillis, *Thermal Radiation in Disperse Systems: An Engineering Approach* (Begell House, 2010).
25. R. Siegel and C. M. Spuckler, "Approximate solution methods for spectral radiative transfer in high refractive index layers," Int. J. Heat Mass Transfer **37**, 403–413 (1994).
26. L. A. Dombrovsky, J. H. Randrianalisoa, W. Lipiński, and D. Baillis, "Approximate analytical solution to normal emittance of semi-transparent layer of an absorbing, scattering, and refracting medium," J. Quant. Spectrosc. Radiat. Transfer **112**, 1987–1994 (2011).
27. H. M. Ã. Shabana, "Determination of film thickness and refractive index by interferometry," Polym. Test. **23**, 695–702 (2004).
28. L. A. Dombrovsky, D. Baillis, and J. H. Randrianalisoa, "Some physical models used to identify and analyze infrared radiative properties of semi-transparent dispersed materials," J. Spectosc. Dynamics **1**, 1–20 (2011).
29. L. Dombrovsky, S. Lallich, F. Enguehard, and D. Baillis, "An effect of "scattering by absorption" observed in near-infrared properties of nanoporous silica," J. Appl. Phys. **107**, 083106 (2010).
30. H. C. Van de Hulst, *Light Scattering by Small Particles* (Wiley, 1957).
31. C. F. Bohren and D. R. Huffman, *Absorption and Scattering of Light by Small Particles* (Wiley, 1983).
32. C. L. Tien and B. L. Drolen, "Thermal radiation in particulate media with dependent and independent scattering," in *Annual Review of Numerical Fluid Mechanics and Heat Transfer* (Hemisphere, 1987), Vol. **1**, pp. 1–32.
33. A. A. Kokhanovsky, *Optics of Light Scattering Media: Problems and Solutions*, 3rd ed. (Praxis, 2004).
34. M. I. Mishchenko, L. D. Travis, and A. A. Lacis, *Multiple Scattering of Light by Particles: Radiative Transfer and Coherent Backscattering* (Cambridge University, 2006).
35. L. Dombrovsky, J. Randrianalisoa, and D. Baillis, "Infrared radiative properties of polymer coatings containing hollow microspheres," Int. J. Heat Mass Transfer **50**, 1516–1527 (2007).
36. R. Guzzi and R. Rizzi, "Water vapor absorption in the visible and near infrared: results of field measurements," Appl. Opt. **23**, 1853–1861 (1984).